

A SCUBA survey of L1689 – the dog that didn’t bark

D. Nutter^{1*}, D. Ward-Thompson¹, P. André²

¹*Department of Physics and Astronomy, Cardiff University, 5 The Parade, Cardiff, CF24 3YB*

²*CEA, DSM, DAPNIA, Service d’Astrophysique, C.E. Saclay, F-91191 Gif-sur-Yvette Cedex, France*

5 February 2008

ABSTRACT

We present submillimetre data for the L1689 cloud in the ρ Ophiuchi molecular cloud complex. We detect a number of starless and prestellar cores and protostellar envelopes. We also detect a number of filaments for the first time in the submillimetre continuum that are parallel both to each other, and to filaments observed in the neighbouring L1688 cloud. These filaments are also seen in the ^{13}CO observations of L1689. The filaments contain all of the star-formation activity in the cloud. L1689 lies next to the well studied L1688 cloud that contains the ρ Oph-A core. L1688 has a much more active star-formation history than L1689 despite their apparent similarity in ^{13}CO data. Hence we label L1689 as the dog that didn’t bark. We endeavour to explain this apparent anomaly by comparing the total mass of each cloud that is currently in the form of dense material such as prestellar cores. We note firstly that L1688 is more massive than L1689, but we also find that when normalised to the total mass of each cloud, the L1689 cloud has a much lower percentage of mass in dense cores than L1688. We attribute this to the hypothesis of Loren (1989) that the star formation in the ρ Ophiuchi complex is being affected and probably dominated by the external influence of the nearby Upper Scorpius OB association and predominantly by σ Sco. L1689 is further from σ Sco and is therefore less active. The influence of σ Sco appears nonetheless to have created the filaments that we observe in L1689.

Key words: stars: formation – stars: pre-main-sequence – ISM: clouds – ISM: dust,extinction – ISM individual: L1689, L1688

1 INTRODUCTION

The earliest stages of low-mass ($0.2\text{--}2M_{\odot}$) star formation are becoming reasonably well understood (see e.g. André, Ward-Thompson, & Barsony 2000 for a review). The prestellar core stage (Ward-Thompson et al. 1994) is the phase in which a molecular cloud core has become gravitationally bound. Thereafter gravitational collapse sets in and a central hydrostatic protostar forms, which is known as a Class 0 protostar (André, Ward-Thompson, & Barsony 1993). Once half of the final mass has accreted onto the central object it is known as a Class I protostar (Wilking, Lada, & Young 1989), and it subsequently evolves through the Class II & III young stellar object (YSO) phases (Lada 1987). Debate continues over the details of this evolutionary process, and different molecular clouds appear to be evolving according to a different interplay of physical mechanisms. These include magnetic fields, turbulence and feedback from previous episodes of star formation. Submillimetre studies of different star-forming regions are required

to help clarify the evolutionary process and determine the effect of these mechanisms.

The L1689 molecular cloud is part of the ρ Ophiuchi molecular cloud complex, which is located at a distance of 128 ± 12 pc from the sun (Bertout, Robichon, & Arenou 1999). It was first detected by Lynds (1962) in a large study of the dark nebulae detected in the Palomar Observatory Sky Survey plates. The ρ Ophiuchi complex was extensively mapped by Loren (1989) using ^{13}CO at a resolution of 2.4 arcmin. The resulting map of the cloud is shown in Fig. 1. The data show that the molecular cloud is composed of a number of sub-clouds, the most massive of which is L1688.

The majority of studies of the ρ Ophiuchi molecular cloud to date have concentrated on the L1688 sub-cloud, also known as the ρ Oph main cloud. A number of filamentary clouds (L1709, L1740, L1744, L1755 and L1765) extend from L1688 in a north easterly direction, and are often called the streamers or the cobwebs of Ophiuchus. To the south-east of L1688 lies L1689, which also has filamentary clouds (L1712 and L1729) extending in roughly the same direction. Loren (1989) measured masses for L1688 and L1689 of $1447 M_{\odot}$ and $566 M_{\odot}$ respectively, while the components of the streamers have lower masses of $100\text{--}300 M_{\odot}$ each. The di-

* E-mail: David.Nutter@astro.cf.ac.uk

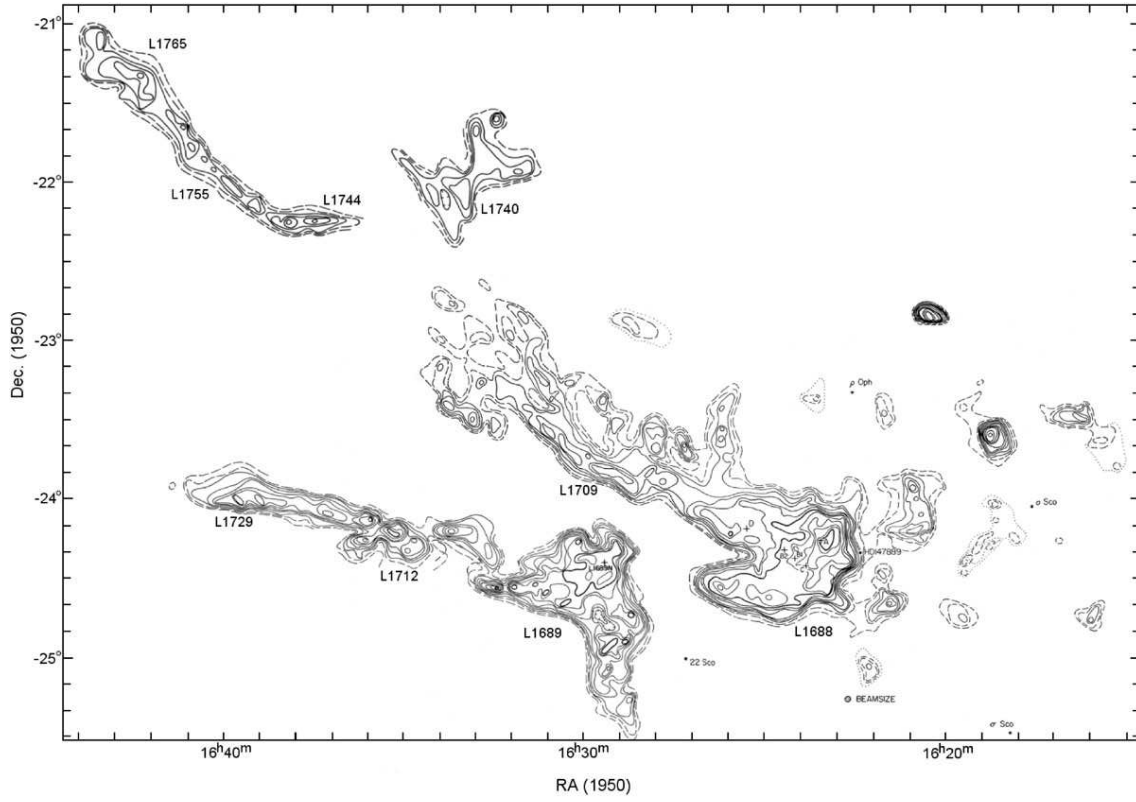


Figure 1. ^{13}CO map of the ρ Ophiuchi complex, from Loren (1989). The contour levels give antenna temperatures $T_R^*(^{13}\text{CO})$ of 4, 5, 6, 7, 8, 10, 12, 14, 18 and 20 K. The names of the clouds are marked.

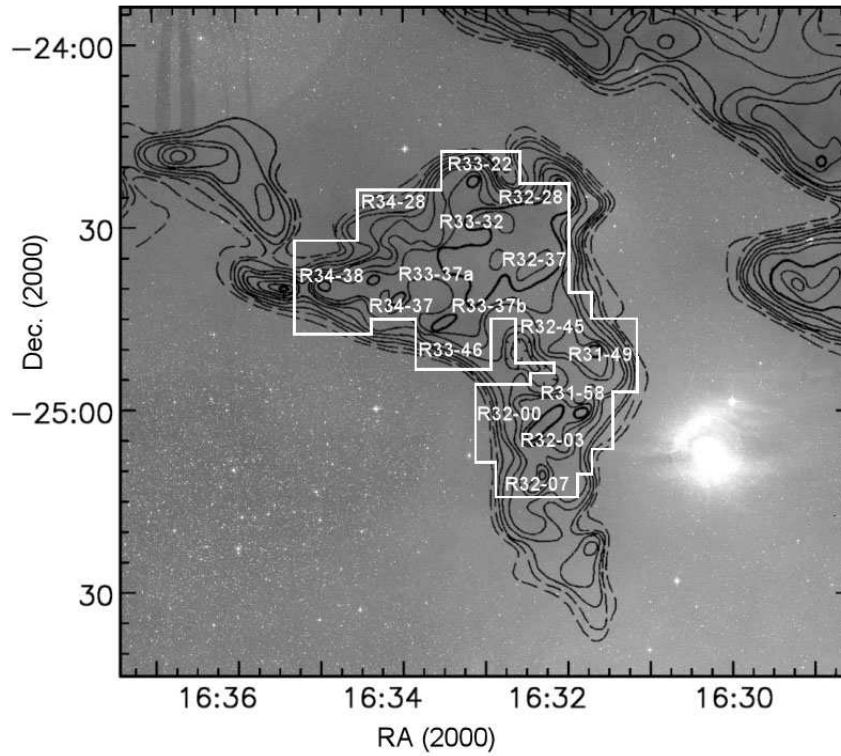


Figure 2. A composite map of the L1689 cloud showing the scan-mapped fields (white outline and labels). The background $0.5\ \mu\text{m}$ image is taken from the Digital Sky Survey, obtained using the *SkyView* interface. The contours are ^{13}CO emission at $T_R^*(^{13}\text{CO})$ of 4, 5, 6, 7, 8, 10, 12, 14, 18 and 20 K (Loren 1989).

Table 1. The positions of each of the scan-mapped fields in the L1689 molecular cloud. The atmospheric conditions during each observation are indicated by the 850 μm zenith optical depth listed in column 5. The field names correspond to those shown in Fig. 2.

Field Name	Map centre		UT Date	$\tau_{850\mu\text{m}}$
	RA (2000)	Dec. (2000)		
R31-49	16:31:39.6	−24:49:43	1999-Mar-09	0.34
—	—	—	2000-Apr-09	0.26
R31-58	16:31:56.7	−24:58:52	1999-Mar-09	0.38
—	—	—	2000-Apr-10	0.22
R32-45	16:32:11.5	−24:45:21	2000-Apr-09	0.22
R32-03	16:32:14.1	−25:03:10	1999-Aug-08	0.22
—	—	—	1999-Aug-09	0.38
R32-07	16:32:22.7	−25:07:50	1999-Apr-08	0.22
—	—	—	2000-Apr-10	0.18
R32-37	16:32:26.1	−24:37:20	2000-Apr-09	0.22
R32-28	16:32:27.6	−24:28:25	1999-Mar-09	0.30
R32-00	16:32:38.8	−25:00:49	2000-Apr-10	0.18
R33-22	16:33:01.9	−24:22:17	2000-Apr-12	0.30
R33-37b	16:33:02.1	−24:37:17	1999-Aug-09	0.26
—	—	—	2000-Apr-11	0.22
R33-32	16:33:17.0	−24:32:16	1999-Mar-09	0.34
—	—	—	2000-Apr-10	0.18
—	—	—	2000-Apr-12	0.30
R33-46	16:33:22.3	−24:46:16	2000-Apr-12	0.30
R33-37a	16:33:38.1	−24:37:15	2000-Apr-11	0.22
R34-28	16:34:01.9	−24:28:13	1999-Mar-09	0.38
—	—	—	1999-Aug-08	0.26
R34-37	16:34:14.1	−24:37:13	2000-Apr-11	0.22
R34-38	16:34:50.2	−24:38:04	1999-Aug-08	0.26
—	—	—	1999-Aug-09	0.30
—	—	—	2000-Apr-11	0.22

rection of the streamers turns to the south at the positions of both L1688 and L1689, forming a horseshoe shape in the case of L1688 and a boomerang shape in the case of L1689 (see Fig. 1).

Numerous studies of the L1688 cloud have revealed a rich history of star formation. Prompted by the association of early-type stars with the ρ Ophiuchi dark cloud, Grasdalen, Strom, & Strom (1973) surveyed the cloud at 2 μm and discovered a large number of embedded young stars. Subsequent observations at a variety of wavelengths (e.g. Wilking & Lada 1983; Andre, Montmerle, & Feigelson 1987; Ward-Thompson et al. 1989; Wilking et al. 1989; Greene et al. 1994; Casanova et al. 1995; Motte, André, & Neri 1998; Johnstone et al. 2000; Johnstone, Di Francesco & Kirk 2004) have revealed large numbers of objects at every stage of star formation. Indeed, studies of this region have greatly increased our knowledge of the star-formation process as a whole.

In contrast, the L1689 cloud appears to have relatively little star-forming activity, concentrated in a small number of isolated sources such as IRAS 16293-2422 (Loren, Wootten, & Wilking 1990). As such, we have labelled L1689 ‘the dog that didn’t bark’. In this paper, we endeavour to find out why there is such an apparent discrepancy between the star-formation activity in L1688 and L1689 when they appear so similar in CO maps – see Fig. 1. We report on submillimetre observations of L1689 and compare them with those taken at other wavelengths, in order

to understand the similarities and differences between L1688 and L1689.

2 OBSERVATIONS

The observations were carried out using the Submillimetre Common User Bolometer Array (SCUBA) on the James Clerk Maxwell Telescope (JCMT). This instrument takes observations at 450 and 850 μm simultaneously through the use of a dichroic beam-splitter. The telescope has a resolution of 8 arcsec at 450 μm and 14 arcsec at 850 μm .

Observations of L1689 were carried out over several nights between 1999 March and 2000 April using the scan-map observing mode as listed in Table 1. A scan-map is made by scanning the array across the sky. The scan direction is 15.5° from the axis of the array in order to achieve Nyquist sampling. The array is rastered across the sky to build up a map several arcminutes in extent.

Time-dependent variations in the sky emission were removed by chopping the secondary mirror at 7.8 Hz. Due to a scan-map being larger in size than the chop throw, each source in the map appears as a positive and a negative source. In order to remove this dual-beam function, each region is mapped six times, with chop throws of 30, 44 and 68 arcsec in both RA and Dec (Emerson 1995). The dual-beam function is removed from each map in Fourier space by dividing each map by the Fourier transform of the dual-beam

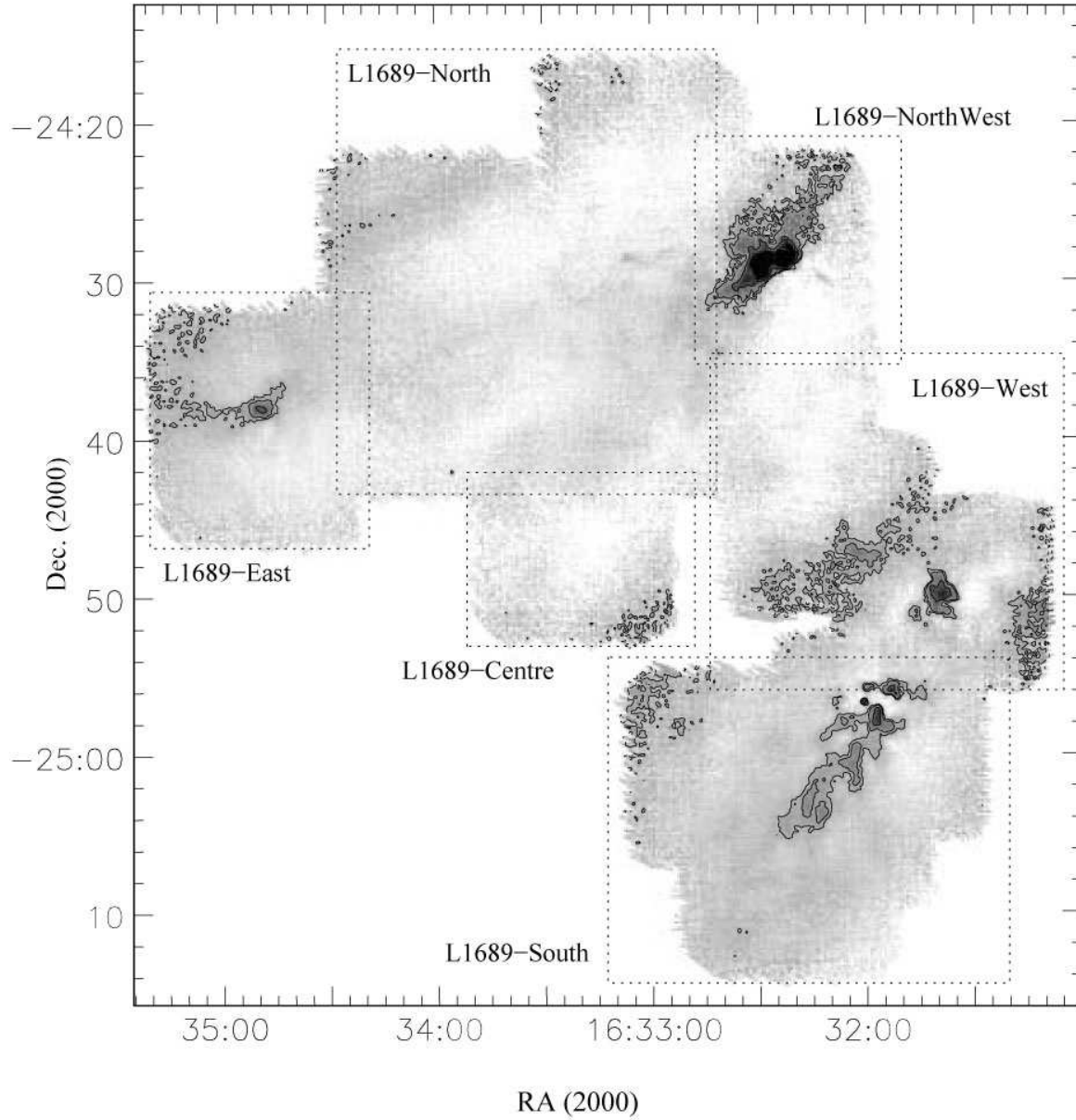


Figure 3. The L1689 cloud at 850 μm . The contour levels are at 3σ , 5σ , 10σ , 20σ , 40σ and 80σ , where σ is the mean noise level over the whole of the map, equal to 20 mJy/beam. Contours are based on the map smoothed to a resolution of 18 arcsec. The map regions in Table 2 are shown as dotted lines.

Table 2. Table showing the noise levels for each region of the L1689 maps. The position of each of the regions is illustrated in Fig. 3.

Region Name	Region Centre		1σ noise (Jy/beam)	
	RA (2000)	Dec. (2000)	850 μm	450 μm
L1689-West	16:31:40	-24:50:00	0.029	2.4
L1689-South	16:32:10	-25:03:00	0.016	0.51
L1689-NorthWest	16:32:30	-24:35:00	0.047	3.4
L1689-Centre	16:33:20	-24:47:00	0.034	1.3
L1689-North	16:33:30	-24:33:00	0.023	0.87
L1689-East	16:34:50	-24:38:00	0.015	0.39

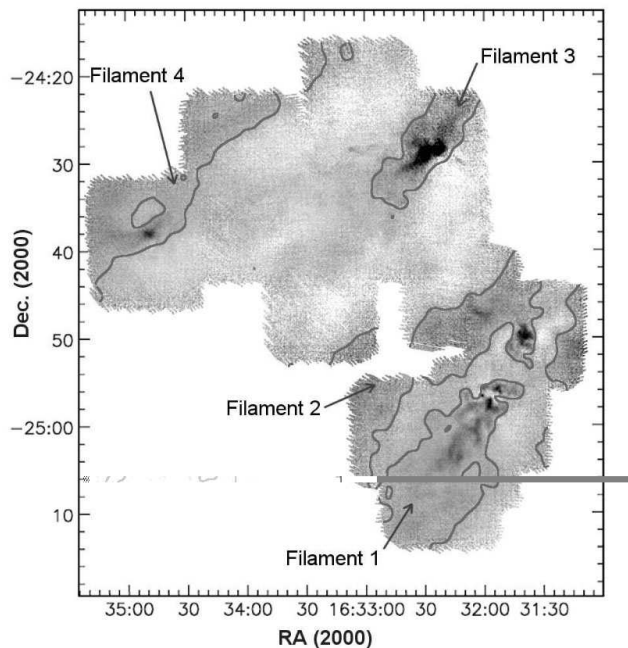


Figure 4. Composite map showing the 850 μm scan-map of L1689 as a grey-scale. The superposed contours are the 850- μm data smoothed to a resolution of 1 arcmin to highlight the large-scale structure. The names of the filaments are also marked (see text for details).

function, which is a sinusoid. The multiple chop-throws allow for cleaner removal of the dual beam function in Fourier space. The maps are then combined, weighting each map to minimise the noise introduced at the spatial frequencies that correspond to zeroes in the sinusoids. Finally the map is converted back into normal space, where it no longer contains the negative sources (Jenness & Lightfoot 2000).

The submillimetre zenith opacity at 450 and 850 μm was determined using the ‘skydip’ method and by comparison with polynomial fits to the 1.3 mm sky opacity data, measured at the Caltech Submillimeter Observatory (Archibald et al. 2002). The average zenith optical depth at 850 μm is listed in Table 1 for each observation. The telescope pointing was checked at regular intervals throughout the nights using planets, secondary calibrators and standard pointing sources.

The data were reduced in the normal way using the SCUBA User Reduction Facility (Jenness & Lightfoot 2000). Calibration was performed using observations of the planet Uranus taken during each shift. We estimate that the absolute calibration uncertainty is $\pm 10\%$ at 850 μm and $\pm 30\%$ at 450 μm , based on the consistency and reproducibility of the calibration from map to map.

3 RESULTS

The map of L1689 is made up of a number of scan-maps, each of which is 12×12 arcmin in size. The positions of the scan-maps were chosen to trace the ^{13}CO emission mapped by Loren (1989). This is shown graphically in Fig. 2, where the mapped area is overlaid in white on the black ^{13}CO

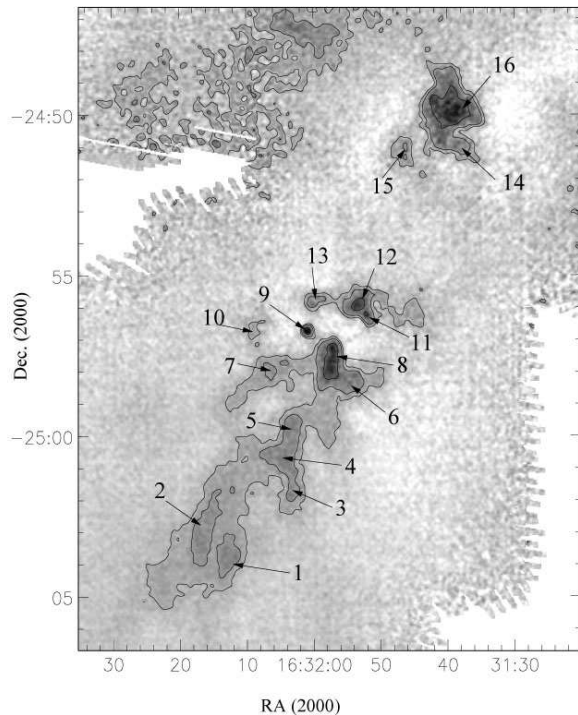


Figure 5. An enlarged view of Filament 1 at 850 μm . The sources SMM 1 – 16 that are associated with this filament are labelled.

contours (Loren 1989). The names and approximate positions of the different scan-map fields are shown in white. The background 0.5 μm image is taken from the Digitized Sky Survey (Lasker 1994), obtained using the *SkyView* interface (McGlynn & Scolick 1994). The mapping strategy was to offset each scan-map from the neighbouring maps by approximately half a map-length. This was to avoid potential ‘striping’ caused by the increased noise levels at the scan-map edges. The name of each scan-map is taken from the J2000 coordinates of the scan-map centre. The observation details are summarised in Table 1.

Fig. 3 shows the data for the L1689 cloud at 850 μm . The area covered is approximately 0.5 deg^2 , which at a distance of 128 pc is equal to $\sim 2.5 \text{ pc}^2$. As a result of the different weather conditions at the telescope when the maps were made, and also the varying integration time per point, the noise level varies across the map. We have therefore split the map up into a number of regions, and measured the mean 1σ noise level for each region. These are given in Table 2. The extent of the different regions, and our names for them, are illustrated with dashed lines in Fig. 3.

A number of sources are seen in the 850 μm map. We have labelled these SMM 1–21 in order of increasing declination. The sources were identified by eye by selecting regions of flux density greater than $4\text{-}\sigma$ above the background level. All the sources are smaller than $\sim 1\text{--}2$ arcmin. Any structure larger than this scale is deemed to be part of the filamentary structure of the cloud, and is discussed below. The identities of the relatively compact (i.e. ≤ 1 arcmin) sources are discussed in the following section. The only source detected at 450 μm is the well-studied binary/multiple Class 0 protostar IRAS 16293-2422 (Wootten 1989; Mundy et al. 1992; Walker, Carlstrom, & Bieging 1993).

Table 3. The position and measured flux density of each source in the L1689 scan-maps at 850 μm and 450 μm . Column 4 indicates whether or not the core is extended in the 14 arcsec 850 μm JCMT beam. The peak flux density is quoted for all sources (columns 7 and 9), with 3σ upper limits given for undetected sources. The integrated flux density within an aperture is given for extended sources in columns 8 and 10. The semi-major & semi-minor axes of these apertures are given in columns 5 and 6. The names given to these sources in other surveys are given in Table 4.

Source Name	RA (2000)	Dec. (2000)	Ext.	Aperture		850 μm		450 μm	
				Semi-major (arcsec)	Semi-minor (arcsec)	Peak (Jy/beam)	Int. (Jy)	Peak (Jy/beam)	Int. (Jy)
SMM 1	16:32:12.5	-25:03:53	Y	32	24	0.15	0.75	< 1.5	–
SMM 2	16:32:16.1	-25:02:44	Y	67	29	0.14	1.6	< 1.5	–
SMM 3	16:32:02.7	-25:01:48	Y	24	22	0.15	0.50	< 1.5	–
SMM 4	16:32:04.1	-25:00:53	Y	38	22	0.18	1.1	< 1.5	–
SMM 5	16:32:03.0	-24:59:48	Y	37	22	0.15	0.67	< 1.5	–
SMM 6	16:31:54.6	-24:58:22	Y	30	20	0.22	0.94	< 1.5	–
SMM 7	16:32:06.3	-24:58:01	Y	41	27	0.11	0.49	< 1.5	–
SMM 8	16:31:57.5	-24:57:40	Y	43	25	0.30	1.4	< 1.5	–
SMM 9	16:32:01.0	-24:56:44	N	13	13	0.44	–	< 1.5	–
SMM 10	16:32:08.6	-24:56:41	Y	39	27	0.11	0.45	< 1.5	–
SMM 11	16:31:52.2	-24:56:13	Y	17	15	0.29	0.56	< 1.5	–
SMM 12	16:31:53.7	-24:55:54	Y	36	21	0.32	1.4	< 1.5	–
SMM 13	16:32:00.3	-24:55:53	Y	31	21	0.23	0.72	< 1.5	–
SMM 14	16:31:37.5	-24:51:09	Y	36	26	0.27	1.5	< 7.1	–
SMM 15	16:31:46.8	-24:51:10	Y	34	27	0.20	1.2	< 7.1	–
SMM 16	16:31:39.2	-24:49:48	Y	63	51	0.40	7.8	< 7.1	–
SMM 17	16:33:55.7	-24:42:06	N	12	11	0.21	–	< 2.6	–
SMM 18	16:34:48.4	-24:38:04	Y	43	30	0.24	2.0	< 1.2	–
SMM 19	16:32:29.3	-24:29:13	Y	48	33	1.64	12	< 10	–
SMM 20	16:32:23.0	-24:28:40	Y	39	28	15.9	28	80	180
SMM 21	16:33:06.2	-24:28:38	Y	27	19	0.12	0.36	< 2.6	–

Table 3 gives the measured flux density for each source detected in the map. The peak flux density is given in Jy/beam for each source at both 450 and 850 μm . 3σ upper limits are given for sources that are undetected at 450 μm . The integrated flux density is also given for sources that are extended in the 14 arcsec JCMT beam. The semi-major and semi-minor axes of the elliptical apertures used to measure these integrated flux densities are given in columns 5 and 6 of Table 3.

Taking the map as a whole, we see that the cloud appears to be composed of a number of approximately parallel filaments, that run the length of the map. These are highlighted in Fig. 4, where the contours are the data after it has been smoothed to a resolution of 1 arcmin to illustrate the large scale structure. A number of sources associated with these filaments are also detected. The nature of these sources is discussed below.

Filament 1 lies at the southern end of the map, and extends northwest-southeast (NW-SE) through the L1689-West and L1689-South regions. The filament appears to have fragmented into a number of objects, forming more than one object across its width in some cases. The degree of fragmentation appears to be greater at the north of the filament, where the majority of the sources detected in this filament are found. The sources at the southern end of the filament are also seen to be less centrally condensed. Fig. 5 shows this filament in more detail. The 16 sources in the filament have been labelled. Most of these objects are significantly extended in the JCMT beam, and have a fairly

complex structure. This filament contains the majority of the sources that are seen in the L1689 molecular cloud.

Filament 2 runs roughly parallel to Filament 1 but slightly to the north, also in a NW-SE direction. There are no detected sources associated with this filament. The filament has been independently detected on a number of scan-maps. Unfortunately, Filament 2 has not been covered very well by the scan-mapping strategy. There is an area that has not been mapped in the middle of the filament, and most of the area that has been mapped has been covered only once. In addition, the filament has mostly been caught on the edges of the scan-maps, where the noise levels can be of order $1.5\times$ higher. As a result of these factors, the level of noise along the filament is higher than average. We therefore suggest that this filament be re-mapped to confirm our findings.

Filament 3 extends from the L1689-NorthWest region, in a NW-SE direction also roughly parallel to Filament 1. The brightest source in this filament is the IRAS 16293 binary/multiple Class 0 protostar (labelled here SMM 20). There is also a weaker source 90 arcsec (approximately 14000 AU) to the southeast of IRAS 16293, named 16293E (SMM 19). It is interesting to note that the extended emission surrounding IRAS 16293 lies parallel to the axes of the other filaments in the map. The filament is only detected in the northwest of the image, though if the line of the filament is extrapolated, a weak unresolved source (SMM 17) is detected at RA (2000) = $16^{\text{h}}33^{\text{m}}55.7^{\text{s}}$, Dec. (2000) = $-24^{\circ}42'06''$.

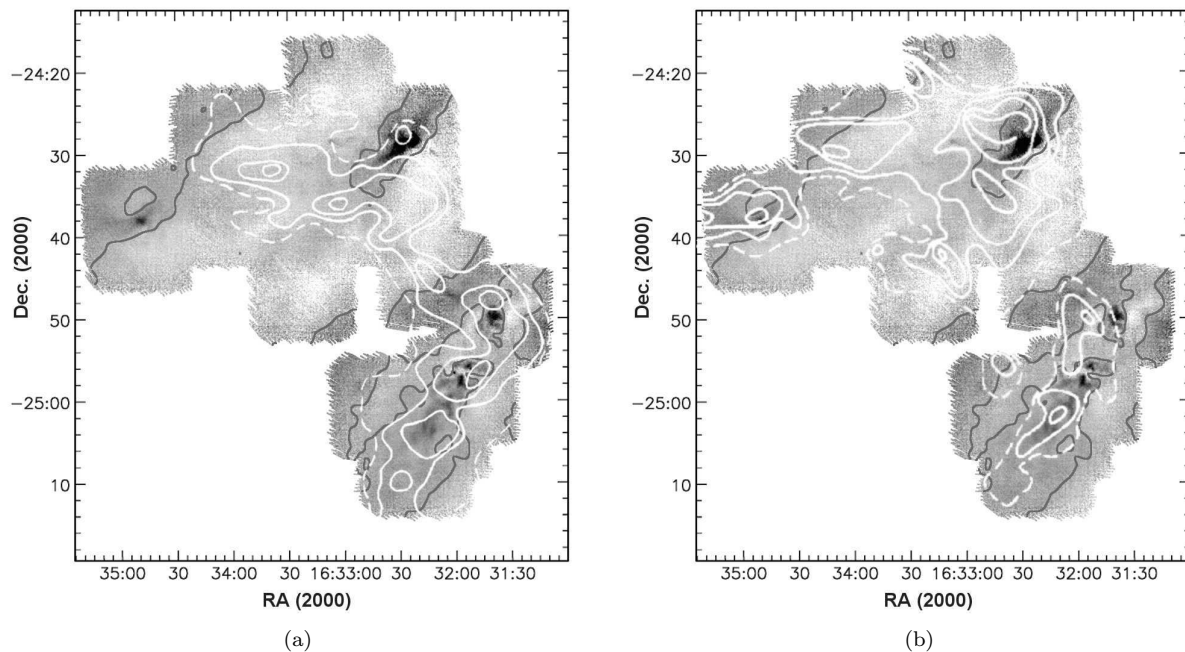


Figure 6. Composite map showing the 850 μm scan-map of L1689 as a grey-scale. The dark contours are 850- μm data smoothed to a resolution of 1 arcmin to highlight the large-scale structure. The light contours are ^{13}CO emission with V_{SLR} of (a) $4.68 - 5.02 \text{ km s}^{-1}$ and (b) $3.32 - 3.66 \text{ km s}^{-1}$ (Loren 1989), and give antenna temperatures $T_R^*(^{13}\text{CO})$ of 2, 4, 6, 8, 10 and 12 K. The continuum filaments can be seen at different velocities in the ^{13}CO data.

Filament 4 extends from the L1689-East region at the east of the map, in a NW-SE direction. Like Filament 2, it skirts along the edge of the map, therefore the noise is higher than average. The only object detected in the filament is the L1689B (Myers & Benson 1983) prestellar core (Ward-Thompson et al. 1994; Kirk, Ward-Thompson, & André 2005) at $\text{RA} (2000) = 16^{\text{h}}34^{\text{m}}48.^{\text{s}}$, $\text{Dec.} (2000) = -24^{\circ}38'00''$, that we label here SMM 18. Filament 4 is the least completely mapped of the four filaments, but it is seen in more than one overlapping scan-map. We also note that the envelope of L1689B is elongated parallel with the filament axis.

When observed with molecular line tracers, the ρ Ophiuchi cloud is also filamentary in appearance (Loren 1989). This filamentary structure is not restricted to the streamers that extend to the northeast, but is also seen in the larger L1688 and L1689 sub-clouds (Wilking & Lada 1983; Loren 1989).

To illustrate this, Figs 6(a)&(b) show our 850 μm data smoothed to highlight the filaments as in Fig. 4. ^{13}CO maps are overlaid as light contours (Loren 1989). Figs. 6(a)&(b) show the ^{13}CO radial velocity intervals $4.68 - 5.02 \text{ km s}^{-1}$ and $3.32 - 3.66 \text{ km s}^{-1}$ respectively. As can be seen, Filament 1 is clearly detected in ^{13}CO at both of these velocity intervals. Filaments 3 and 4 and the northern half of Filament 2 are seen at velocities $3.32 - 3.66 \text{ km s}^{-1}$ (Fig. 6b).

4 INDIVIDUAL SOURCES

4.1 Identities of the detected sources

In identifying the nature of submillimetre detected sources, there are a number of factors to take into account. To differ-

entiate between a prestellar core and a Class 0 protostar, one can look for a centimetre radio source or a collimated molecular outflow, which would indicate the presence of a central hydrostatic object. Class 0 protostars are distinguished from more evolved classes of protostar by a large ratio of submillimetre to bolometric luminosity, or the presence of a centrally peaked and extended envelope (André et al. 2000). More evolved protostars (Class I and later) can be seen in the infrared. In this section, we discuss the identities of each of the sources, and summarise the source parameters in Table 4.

In order to estimate whether or not the sources are gravitationally bound, we compare their masses to the Bonnor-Ebert critical mass $M_{BE} = 2.4Ra_s^2/G$ (Bonnor 1956; Ebert 1955), where R is the radius of the source (taken to be the geometric mean of the semi-major and semi-minor axes given in Table 3), a_s is the isothermal sound speed, and G is the gravitational constant.

The source SMM 1 corresponds to the prestellar core L1689A, which has previously been mapped in the submillimetre (Kirk et al. 2005) and also in the far-infrared (Ward-Thompson, André, & Kirk 2002). This core's position, close to the leading edge of the L1689 cloud nearest the Upper Scorpius OB association (see Section 5.3), could potentially explain the unusual temperature profile measured in the far-infrared by Ward-Thompson et al. (2002).

The sources SMM 2-5 are all fairly extended cores that are not very centrally peaked. Their masses are comparable with the Bonnor-Ebert critical mass, as given in Table 4. These sources have not been observed previously, with the exception of SMM 5 which was detected in the millimetre (André & Montmerle 1994), and possibly corresponds to the source VLA 16289, though the nature of this object is unknown. SMM 7 is also extended, though its mass

Table 4. The prestellar core masses and protostellar envelope masses for the SCUBA detections in L1689. The assumed values of the temperature and the dust opacity for each of the sources is listed in columns 3 & 4 (see text for details). The Bonnor-Ebert critical mass for the starless cores is given in column 6. The region of the cloud that each source is associated with is included in column 7. *IRAS 16293 is known to be a binary/multiple system. References in column 8 are as follows: ¹Bacmann et al. 2000, ²Greene et al. 1994, ³Bontemps et al. 2001, ⁴Kirk et al. 2005, ⁵André & Montmerle 1994, ⁶Mundy et al. 1992, ⁷Castets et al. 2001, ⁸Martin et al. 1998, ⁹André et al. 1996.

Source Name	Class	Temp (K)	κ_{850} (cm^2g^{-1})	Mass (M_{\odot})	M_{BE} (M_{\odot})	^{13}CO region	Other Names
SMM 1	Prestellar	12	0.01	0.3	0.4	R55	L1689A ⁴
SMM 2	Prestellar	12	0.01	0.6	0.7	R55	
SMM 3	Prestellar	12	0.01	0.2	0.3	R55	
SMM 4	Prestellar	12	0.01	0.4	0.4	R55	
SMM 5	Prestellar	12	0.01	0.3	0.4	R55	
SMM 6	Prestellar	12	0.01	0.4	0.4	R55	
SMM 7	Starless	12	0.01	0.2	0.5	R55	
SMM 8	Prestellar	12	0.01	0.6	0.5	R55	L1689SMM ⁴
SMM 9	I	30	0.02	0.02	–	R55	IRAS 16289-2450, L1689-IRS6 ² , ISO-209 ³ , L1689S-IRS67 ⁴
SMM 10	Starless	12	0.01	0.2	0.5	R55	
SMM 11	II	30	0.03	0.02	–	R55	L1689-IRS5 ² , ISO-204 ³
SMM 12	Prestellar	12	0.01	0.6	0.4	R55	
SMM 13	Prestellar	12	0.01	0.3	0.4	R55	
SMM 14	Prestellar	12	0.01	0.6	0.5	R53	
SMM 15	Prestellar	12	0.01	0.5	0.5	R53	R53 ¹
SMM 16	Prestellar	12	0.01	3.0	0.8	R53	R53 ¹
SMM 17	II	30	0.03	0.01	–	R65	RX J1633.9-2442 ⁸
SMM 18	Prestellar	12	0.01	0.8	0.5	R65	L1689B ⁹
SMM 19	0	30	0.02	0.6	–	R57	IRAS 16293-2422E ⁷
SMM 20	0*	30	0.02	1.3	–	R57	IRAS 16293-2422 ⁶
SMM 21	Starless	12	0.01	0.1	0.3	R57	

is less than half of its Bonnor-Ebert critical mass. Therefore this source may well not be bound, but a transient object. Hence we label it as starless rather than prestellar in Table 4. This follows the distinction of definitions made by Ward-Thompson et al. (2006), who stated that the difference between a starless core and a prestellar core is that a prestellar core should be consistent with being gravitationally bound.

SMM 8 is the prestellar core L1689SMM, which was mapped by Kirk et al. (2005) using SCUBA in jiggle-map mode. There is no evidence of a protostar at the centre. The core is elongated in a north-south direction, though shows no evidence of fragmenting along its length. Both the morphology and flux density of our data are consistent with the earlier jiggle-map. There is a weaker source (SMM 6) to the south-west of SMM 8, which partially overlaps it.

SMM 9 is the Class I protostar IRAS 16289-2450. It has also been detected at a number of wavelengths from the near-infrared (L1689-IRS6 – Greene et al. 1994), the mid-infrared (ISO-209 – Bontemps et al. 2001) and the millimetre (L1689S-IRS67 – André & Montmerle 1994). This object is centrally condensed in the submillimetre and no extended emission is detected.

There is an abrupt gap in the filament between SMM 8 and the group of objects to the north (SMM 11, 12 and 13). This could be caused by the gravitational collapse of the filament onto the surrounding cores, or the cavity could have been cleared by outflows from IRAS 16289-2450 (SMM 9), which lies within the cavity.

SMM10 is similar in appearance to its neighbour, SMM 7, and also appears not to be bound. SMM 11 is a Class II protostar which has previously been identified in the near-infrared (L1689-IRS5 – Greene et al. 1994) and mid-infrared (ISO-204 – Bontemps et al. 2001). Approximately 25 arcsec north of this (0.015 pc) lies SMM 12, which has not been previously observed at other wavelengths. This object is assumed to be prestellar in nature. SMM 13 has also not been detected at other wavelengths. Its mass is $\sim 70\%$ of the critical Bonnor-Ebert mass, therefore it may not be bound. Again we label this source as starless in Table 4.

SMM 16 lies at the northern end of Filament 1, and is one of the brighter sources in the map. It appears to have some internal structure, though this is poorly resolved in the 14 arcsec beam. This suggests that SMM 16 could be composed of multiple unresolved sources, surrounded by a common envelope. The diameter of the source is approximately 2 arcmin (0.08 pc at a distance of 130 pc). A VLA survey has been conducted of this region (Stine et al. 1988). However, no centimetre sources coincident with SMM 16 were detected. This indicates that the source (or sources) may be prestellar in nature.

Two sources (SMM 14 & 15) are located 1–2 arcmin from the centre of SMM 16. Again there is no evidence of associated protostars (Stine et al. 1988), we therefore assume that these objects are prestellar, based on their Bonnor-Ebert masses. The three sources SMM 14, 15 and 16 are coincident with the starless core R53 which has been observed in absorption in the mid-infrared (Bacmann et al. 2000).

SMM 17 is a very weak isolated unresolved source, which lies 18 arcsec from the Class II YSO RX J1633.9-2442, which was identified through optical spectroscopy follow-up observations to a ROSAT X-ray survey of ρ Ophiuchi (Martin et al. 1998). It is assumed that the submillimetre emission is associated with this source.

SMM 18 is the well studied prestellar core L1689B (e.g. Kirk et al. 2005, and references therein). This was one of the original starless ammonia cores mapped by Myers & Benson (1983) and subsequently determined to be prestellar in nature (Ward-Thompson et al. 1994). Subsequent mapping with the 1.3 mm MPIfR bolometer array at the IRAM 30m telescope confirmed the results of the earlier survey (André et al. 1996), and provided a more detailed picture of the density profile of the core. The morphology of L1689B, as shown in Fig. 3, is elongated in a roughly east-west direction. This is consistent with the 1.3 mm map (André et al. 1996) and also a SCUBA jiggle-map of the core (Kirk et al. 2005). Ward-Thompson et al. (2002) performed a greybody fit to the SED of L1689B between 90 μ m and 1.3 mm using ISO, JCMT and IRAM data, and found a best-fit temperature of $11.9^{+0.7}_{-0.5}$ K.

The brightest source in the map is SMM 20, which is the binary/multiple Class 0 protostar IRAS 16293. This object has been well studied at a number of wavelengths (e.g. Wootten 1989; Mundy et al. 1992; Walker, Carlstrom, & Bieging 1993; Ceccarelli et al. 1998; Castets et al. 2001; Correia, Griffin, & Saraceno 2004), and is used as a secondary calibrator for submillimetre observations using SCUBA (Sandell 1994). It appears to be a hierarchical system, with two components (16293A1 & A2) separated by 47 AU, and a third source (16293B) located approximately 800 AU to the north-west (Wootten 1989). The objects are Class 0 protostars and are the sources of a quadrupolar molecular outflow, though 16293B shows no evidence of current outflow activity (Walker, Carlstrom, & Bieging 1993). 16293A and B are separated by 5 arcsec and are therefore unresolved in the 14 arcsec JCMT beam. Molecular line studies of species that adsorb to grain surfaces (e.g. Castets et al. 2001; Wakelam et al. 2004) indicate that the envelope of IRAS 16293 is composed of a hot core, approximately 2 arcsec (260 AU) across, at a temperature of ~ 100 K. The core is surrounded by a cooler outer envelope at a temperature of 20 – 30 K.

SMM 19 corresponds to 16293E, which is located approximately 85 arcsec (0.05 pc) to the east of IRAS 16293. Castets et al. (2001) have argued that 16293E is a Class 0 protostar, on the grounds of a detected molecular outflow. Stark et al. (2004) did not detect the outflow from 16293E, and argued that the source is prestellar. This may have been due to a sensitivity effect, so we treat this source as a Class 0.

SMM 21 is a weak source with no previous detections at other wavelengths. Comparison with its Bonnor-Ebert critical mass indicates that it is probably not bound. We label it as a starless core.

4.2 Source Masses

Table 4 summarises the results of the previous section and gives mass estimates for all of the detected sources. The envelope mass M is calculated using:

$$M = \frac{S_{850} D^2}{\kappa_{850} B_{850,T}}, \quad (1)$$

where S_{850} is the 850 μ m flux density, D is the distance to the source, κ_{850} is the mass opacity of the gas and dust, and $B_{850,T}$ is the Planck function at temperature T .

For the starless and prestellar cores in this sample, we assume a value for $\kappa_{1.3\text{mm}}$ of $0.005 \text{ cm}^2 \text{ g}^{-1}$, as recommended by Henning, Michel, & Stognienko (1995), and scale this to 850 μ m using a canonical value of β of 1.5 (André & Montmerle 1994), giving $\kappa_{850\mu\text{m}} = 0.01 \text{ cm}^2 \text{ g}^{-1}$. These values of κ assume a gas-to-dust ratio of 100 (Hildebrand 1983). For the denser envelopes around Class 0 and I protostars, it is assumed that the formation of icy mantles will increase the $\kappa_{1.3\text{mm}}$ by a factor ~ 2 (André & Montmerle 1994; Henning et al. 1995). Again, a canonical β of 1.5 is used, giving a value of $\kappa_{850\mu\text{m}} = 0.02 \text{ cm}^2 \text{ g}^{-1}$ for these classes of object. For the higher density circumstellar disks surrounding Class II YSOs, grain agglomeration will increase $\kappa_{1.3\text{mm}}$ still further (Henning et al. 1995). Beckwith et al. (1990) found that the best fits to the submillimetre spectra of T-Tauri stars are given by $\kappa_{1.3\text{mm}} = 0.02 \text{ cm}^2 \text{ g}^{-1}$ and $\beta = 1$. These values correspond to $\kappa_{850\mu\text{m}} = 0.03 \text{ cm}^2 \text{ g}^{-1}$.

The temperature of 12 K calculated for L1689B (Ward-Thompson et al. 2002) was used for all of the prestellar and starless cores. For protostellar envelopes, the volume averaged dust temperature is assumed to be 30 K (André & Montmerle 1994).

5 COMPARISON OF L1689 WITH L1688

5.1 Cloud constituents

It is interesting to compare the L1688 and L1689 clouds, as they share the same environment, yet previous studies have indicated that L1688 has a much higher level of star formation (e.g. Loren et al. 1990). Loren (1989) measured the mass of L1688 and L1689 from ^{13}CO maps to be 1447 and 566 M_{\odot} respectively, differing by a factor of 2.6. The area on the sky of L1688 (measured at the 6 K contour of the ^{13}CO maps — see Fig. 1) is 1.4 times larger than L1689. Assuming that the two clouds have approximately the same aspect ratio (which is a fair assumption, given their similar morphology), the volume of L1688 is 1.7 times that of L1689. The average density of L1688 is therefore approximately 1.5 times larger than that of L1689. As a result of this, we might expect star formation in L1688 to proceed more rapidly than in L1689.

Loren (1989) divided the two clouds into 89 different regions, which have a clear spatial or velocity separation. These regions are used in the following analysis to compare the star-formation activity across the clouds. Fig. 7 shows the region boundaries overlaid on the ^{13}CO contour map. The names of the regions that have been mapped in the submillimetre are marked on Fig. 7 (see below).

Loren et al. (1990) investigated differences in the star-formation rates of the different regions of the ρ Ophiuchi cloud. To do this, they compared the total luminosity (L) of the young stars associated with each region, with the mass (M) of the gas, determined using the ^{13}CO measurements (Loren 1989). They measured values of L/M of

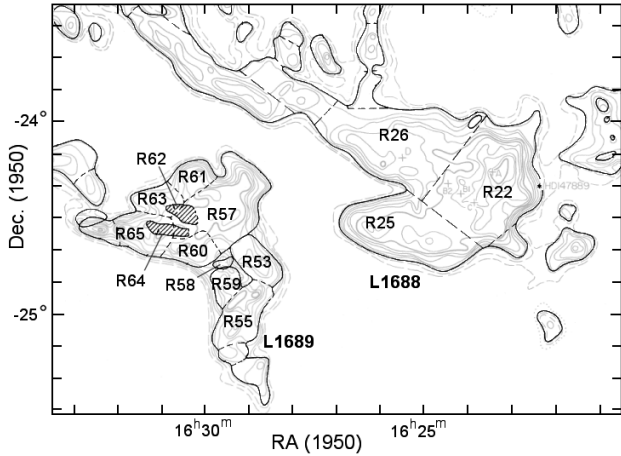


Figure 7. The different regions of L1688 and L1689, defined by spatial or velocity separations (Loren 1989). The region names are marked for areas of the clouds which have been mapped in the submillimetre.

$5.2 L_{\odot}/M_{\odot}$ for L1688 and $0.1 L_{\odot}/M_{\odot}$ for L1689, indicating a much larger star-formation efficiency (SFE) in L1688. This method of estimating the SFE is biased towards high mass stars. Loren et al. (1990) also calculated the ratio N/M , where N is the number of young stars associated with each region. This estimate of the SFE is biased towards low mass stars. They again found that of all of the components of ρ Ophiuchi, L1688 has the highest SFE, with a value of N/M of 0.06. However, the value of N/M of 0.05 for L1689 is only slightly lower.

These methods are both probes of the past star-formation activity in the two clouds. In the following section, we look at the mass of the material currently involved in star formation within each region of the two clouds, in order to compare the current star-formation activity.

5.2 Star-formation efficiency

Johnstone et al. (2000) mapped the densest parts of the L1688 cloud using the SCUBA camera on the JCMT. Together with the data presented here, these make an ideal dataset to compare the current star-formation activity of the two clouds. Johnstone et al. smoothed their map of L1688 by twice the largest chop throw (130 arcsec), and subtracted this from the map. This was done in order to remove all large scale structure, some of which could result from residual atmospheric noise or incorrectly fitted baselines in the data reduction process.

For the purposes of directly comparing the two datasets, we carried out the same step, and subtracted the large scale structure. In the following analysis, all the core masses are calculated assuming a distance to the region of 130 pc, and a dust temperature of 20 K. Again, this is to allow a direct comparison of the two data-sets.

The sensitivities of the two surveys are not significantly different. The SCUBA map of L1688 has a 1σ sensitivity of approximately 10 mJy/beam (Johnstone et al. 2000), compared to our map of L1689, which has a 1σ sensitivity of 15 – 30 mJy/beam (see Table 2).

The SCUBA map of L1689 presented here covers most

Table 5. The masses measured using different tracers for the L1688 and L1689 clouds. The mass of each ^{13}CO region is given in column 3 (Loren 1989). The sum of the masses of all starless and prestellar cores in each of the regions is given in column 4 and simply labelled M_{pre} . These were calculated using the SCUBA data from this study for L1689, and SCUBA data from Johnstone et al. (2000), as well as IRAM 30m data from Motte et al. (1998), for L1688. All the masses quoted in the table have been scaled such that they correspond to an assumed distance of 130 pc and temperature of 20 K. For each ^{13}CO region, the ratio of the prestellar and starless mass to the total mass of the region is given in column 5. The prestellar mass for R26 is calculated using table 2 of Motte et al. (1998). Note the difference of a factor of two between the total $M_{\text{pre}}/M_{^{13}\text{CO}}$ for L1688 and L1689.

Cloud Name	^{13}CO Region	$M_{^{13}\text{CO}}$ (M_{\odot})	M_{pre} (M_{\odot})	$\frac{M_{\text{pre}}}{M_{^{13}\text{CO}}}$
L1688	R22	557	16.4	0.029
	R25	243	0.6	0.002
	R26	136	0.2	0.001
	Total	936	17.2	0.018
L1689	R53	40	1.3	0.033
	R55	55	1.4	0.025
	R57	133	0.1	0.0008
	R58	1	0	0
	R59	15	0	0
	R60	20	0	0
	R61	7	0	0
	R62	7	0	0
	R63	13	0	0
	R64	4	0	0
	R65	26	0.3	0.012
	Total	321		0.010

of the ^{13}CO regions named by Loren (1989) between R53 and R65 (see Table 5 and Figure 7). The area covered by the SCUBA map of L1688 is approximately coincident with R22. The SCUBA map also covers the portion of R25 that is coincident with ρ -Oph F (see Loren & Wootten 1986; Loren et al. 1990). Though this region was not completely mapped by Johnstone et al. (2000), a wider area survey of ρ Ophiuchus (Johnstone et al. 2004) has indicated that there is very little star-formation activity in R25 except that contained in ρ -Oph F.

The SCUBA map of L1688 does not include the ρ -Oph D core in R26, therefore data obtained using the IRAM 30m telescope (Motte et al. 1998) were used to extend the following analysis to this region. Motte et al. separated the IRAM data into large and small scale structure using a wavelet analysis. We use the core masses for their small scale ‘clumps’ (see their table 2), which, like the Johnstone et al. (2000) data, have effectively had the larger scale structure removed. For consistency with the other data-sets, we also scale the R26 core masses to a temperature of 20 K and a distance of 130 pc.

Table 5 gives the mass of each cloud region, measured from the ^{13}CO emission (Loren 1989). The total mass of prestellar and starless cores within each region (M_{pre}) is given in column 4. This is calculated from the submillimetre dust emission from the cores in L1688 (Motte et al. 1998;

Johnstone et al. 2000) and L1689. The cores that contain protostellar sources have not been included in these values. This is so we can evaluate and compare the potential yield of the next generation of star formation in the two clouds.

Table 5 shows that the current star-formation activity is highly variable across both clouds. R22 has the largest mass of dense cores, with $16 M_{\odot}$ compared to $< 2 M_{\odot}$ in each of the regions of L1689. This may be reasonably expected, as the R22 region is significantly more massive than the other regions. In order to compare the fraction of the mass in dense cores in the different regions directly, we divide the mass in cores by the mass of the region, measured from ^{13}CO maps (Loren 1989). This is given for each region in column 5 of Table 5.

When the two clouds (L1688 and L1689) are considered as a whole, L1688 has a much higher fraction (by a factor of 2) of its mass contained in dense cores, with a value of $M_{\text{pre}}/M_{^{13}\text{CO}}$ of 0.018, compared to 0.010 for L1689. Even if we ignore the regions of L1689 that contain no submillimetre cores, and only consider R53, R55, R57 & R65, the total prestellar core mass ratio for L1689 only rises to 0.012. This is still only two-thirds of the value seen in L1688. This indicates that L1688 will probably have a higher star formation efficiency in the next generation of star formation.

However, the values of $M_{\text{pre}}/M_{^{13}\text{CO}}$ for the most active regions of the two clouds (i.e. R22 in L1688 and R53 & R55, which make up Filament 1 in L1689) are in fact similar (although the absolute masses are much smaller in R53 and R55). This could be indicating that parts of L1689 may not be as infertile as was previously thought. We note that these three regions are located at the western edges of L1688 and L1689. We consider the significance of this in the following section.

We finally note that the fraction of prestellar material in ρ -Oph A (see Loren & Wootten 1986; Loren et al. 1990) is an order of magnitude higher than in the rest of R22 (in agreement with Motte et al. 1998). To calculate this, we compared the mass of compact submillimetre condensations in ρ -Oph A (Johnstone et al. 2000) with the mass measured using C^{18}O (see Wilking & Lada 1983, their table 2 and fig. 4).

To summarise this section, we have found that on average, the L1688 cloud has a much higher fraction of its mass in dense cores than L1689. The western edges of both L1688 (R22) and L1689 (filament 1) have comparable fractions. ρ -Oph A is significantly more efficient at converting its mass into dense cores than any other component of the molecular cloud, and it appears likely that the existing young star cluster will continue to grow in richness. The regions to the east of both clouds have a much lower mass fraction in dense cores.

5.3 Sequential star formation

One possible explanation for the picture painted in the previous section is that the star formation in both of the clouds is being affected by an external influence, such as the by-products of nearby young massive stars. This scenario is known as sequential or triggered star formation, and was first suggested by Elmegreen & Lada (1977).

In this picture, the stars which have already formed, interact with the molecular cloud, triggering further star for-

mation, which propagates through the cloud. This scenario has previously been used to explain the star formation in ρ Oph (e.g. Loren & Wootten 1986; Loren 1989). In this case, we believe that the star formation in both L1688 and L1689 is being influenced by members of the Upper Scorpius OB association.

The most massive and luminous nearby component of the Upper Scorpius OB association is σ Sco. This is a hierarchical multiple containing an O9V star and a B2III star and at least two other B stars (e.g. Pigulski 1992). σ Sco lies at a distance of 100 arcmin from L1688 (projected distance 4 pc), and 150 arcmin from L1689 (projected distance 6 pc). It appears to be a prime candidate for the triggering mechanism in both of these clouds.

This hypothesis is consistent with the observation that the majority of the star formation in both clouds is occurring primarily in regions R22, R53 & R55, which make up parallel filaments at the edge of each cloud closest to σ Sco. These filaments are perpendicular to the line of sight joining each cloud and σ Sco. In addition, the extensions of both L1688 and L1689 to the north-east lie on a line directly away from σ Sco (Loren 1989). In this hypothesis, the eastern regions of the two clouds are shielded from the triggering source by the two filaments. We note that R57 is unusual in that it is located on the western edge of L1689, yet has a very small value of $M_{\text{pre}}/M_{^{13}\text{CO}}$. However, R57 has recently formed the protostellar sources SMM 19 & 20, and if the mass associated with these sources is included, then the fertility of R57 becomes comparable with the regions of Filament 1.

The influence of σ Sco has clearly had a different effect on the two clouds, as is evidenced by the young proto-cluster that has formed in L1688, and the lack of such a cluster in L1689. We hypothesise that this difference in star-formation activity in the two clouds is simply due to the fact that L1688 is closer to σ Sco. Hence it suffers a greater effect according to the square of the distance difference.

The sequential star formation in this region can be traced back a number of generations. The Upper Scorpius OB association is adjacent to an older OB association called Upper Centaurus-Lupus. Preibisch & Zinnecker (2001) suggest that the massive stars in Upper Centaurus-Lupus triggered the star formation in Upper Scorpius, just as Upper Scorpius is triggering star formation in ρ Oph. It appears though that this is the end of the line for sequential star formation, as the only massive star to have formed in L1688 or L1689 is the young B3 star S1 (Grasdalen, Strom, & Strom 1973). It is therefore unlikely that this star will have the energy required to propagate the star formation as effectively through the remainder of the ρ Ophiuchi cloud in the same way.

6 CONCLUSIONS

We have mapped the L1689 cloud at submillimetre wavelengths, and detected a number of cores and protostellar envelopes, some of which are reported here for the first time. We have detected filaments in the submillimetre continuum that are also seen in the ^{13}CO observations of the cloud. All of the detected star-formation activity in L1689 is contained within these filaments, the majority being in Filament 1.

We have compared the potential future rate of star for-

mation of L1689 with that of L1688 by looking at the fraction of mass of each cloud that is currently in starless and prestellar cores. We find that when normalised to the total mass of each cloud, the L1688 cloud has on average a much higher percentage of mass in cores. This is consistent with the higher star-formation activity observed in L1688.

We deduce that L1688 and L1689 are both examples of triggered star formation caused by σ Sco and the reason that the L1689 dog has not barked is that it is less massive than L1688 and is further away from σ Sco.

ACKNOWLEDGEMENTS

The authors wish to thank the referee, Doug Johnstone, for comments which improved this manuscript. The authors would also like to thank the staff of the JCMT for assistance with the observations. The JCMT is operated by the Joint Astronomy Centre, Hawaii, on behalf of the UK PPARC, the Netherlands NWO, and the Canadian NRC. DJN acknowledges PPARC for PDRA support.

The Digitized Sky Survey was produced at the Space Telescope Science Institute under U.S. Government grant NAG W-2166. The images of these surveys are based on photographic data obtained using the Oschin Schmidt Telescope on Palomar Mountain and the UK Schmidt Telescope. The plates were processed into the present compressed digital form with the permission of these institutions.

The authors acknowledge the use of NASA's *SkyView* facility (<http://skyview.gsfc.nasa.gov>) located at NASA Goddard Space Flight Center. The authors also gratefully acknowledge R. Loren for permission to use the ^{13}CO maps in Figures 1, 2, 6 and 7.

REFERENCES

- André P., Montmerle T., 1994, *ApJ*, 420, 837
- Andre P., Montmerle T., Feigelson E. D., 1987, *AJ*, 93, 1182
- André P., Ward-Thompson D., Barsony M., 1993, *ApJ*, 406, 122
- André P., Ward-Thompson D., Motte F., 1996, *A&A*, 314, 625
- André P., Ward-Thompson D., Barsony M., 2000, in Mannings V., Boss A., Russell S. S., eds, *Protostars and Planets IV*. Univ. Arizona Press, p. 59
- Archibald E. N., et al., 2002, *MNRAS*, 336, 1
- Bacmann A., André P., Puget J.-L., Abergel A., Bontemps S., Ward-Thompson D., 2000, *A&A*, 361, 555
- Beckwith S. V. W., Sargent A. I., Chini R. S., Guesten R., 1990, *AJ*, 99, 924
- Bertout C., Robichon N., Arenou F., 1999, *A&A*, 352, 574
- Bonnor W. B., 1956, *MNRAS*, 116, 351
- Bontemps S., et al., 2001, *A&A*, 372, 173
- Casanova S., Montmerle T., Feigelson E. D., Andre P., 1995, *ApJ*, 439, 752
- Castets A., Ceccarelli C., Loinard L., Caux E., Lefloch B., 2001, *A&A*, 375, 40
- Ceccarelli C., et al., 1998, *A&A*, 331, 372
- Correia J. C., Griffin M., Saraceno P., 2004, *A&A*, 418, 607
- Ebert R., 1955, *ZA*, 37, 217
- Elmegreen B. G., Lada C. J., 1977, *ApJ*, 214, 725
- Emerson D. T., 1995, in *ASP Conf. Ser. 75, Multifield Systems for Radio Telescopes*, ed. D. T. Emerson & J. M. Payne (San Francisco: ASP), 309
- Grasdalen G. L., Strom K. M., Strom S. E., 1973, *ApJ*, 184, L53
- Greene T. P., Wilking B. A., André P., Young E. T., Lada C. J., 1994, *ApJ*, 434, 614
- Henning T., Michel B., Stognienko R., 1995, *P&SS*, 43, 1333
- Hildebrand R. H., 1983, *QJRAS*, 24, 267
- Jenness T., Lightfoot J.F., 2000, *Starlink User Note* 216, Starlink Project, CCLRC
- Johnstone D., Wilson C. D., Moriarty-Schieven G., Joncas G., Smith G., Gregersen E., Fich M., 2000, *ApJ*, 545, 327
- Johnstone D., Di Francesco J., Kirk H., 2004, *ApJ*, 611, L45
- Kirk J. M., Ward-Thompson D., André P., 2005, *MNRAS*, 360, 1506
- Lada C. J., 1987, *IAUS*, 115, 1
- Lasker B. M., 1994, *IAUS*, 161, 167
- Loren R. B., 1989, *ApJ*, 338, 902
- Loren R. B., Wootten A., 1986, *ApJ*, 306, 142
- Loren R. B., Wootten A., Wilking B. A., 1990, *ApJ*, 365, 269
- Lynds B. T., 1962, *ApJS*, 7, 1
- Martin E. L., Montmerle T., Gregorio-Hetem J., Casanova S., 1998, *MNRAS*, 300, 733
- McGlynn T., Scollick K., 1994, *ASPC*, 61, 34
- Motte F., André P., Neri R., 1998, *A&A*, 336, 150
- Mundy L. G., Wootten A., Wilking B. A., Blake G. A., Sargent A. I., 1992, *ApJ*, 385, 306
- Myers P. C., Benson P. J., 1983, *ApJ*, 266, 309
- Ossenkopf V., Henning T., 1994, *A&A*, 291, 943
- Pigulski A., 1992, *A&A*, 261, 203
- Preibisch T., Zinnecker H., 2001, *ASPC*, 243, 791
- Sandell G., 1994, *MNRAS*, 271, 75
- Stark R., et al., 2004, *ApJ*, 608, 341
- Stine P. C., Feigelson E. D., Andre P., Montmerle T., 1988, *AJ*, 96, 1394
- Wakelam V., Castets A., Ceccarelli C., Lefloch B., Caux E., Pagani L., 2004, *A&A*, 413, 609
- Walker C. K., Carlstrom J. E., Bieging J. H., 1993, *ApJ*, 402, 655
- Ward-Thompson D., André P., Crutcher R. M., Johnstone D., Onishi T., Wilson C., 2006, in: 'Protostars and Planets V', in press
- Ward-Thompson D., André P., Kirk J. M., 2002, *MNRAS*, 329, 257
- Ward-Thompson D., Robson E. I., Whittett D. C. B., Gordon M. A., Walther D. M., Duncan W. D., 1989, *MNRAS*, 241, 119
- Ward-Thompson D., Scott P. F., Hills R. E., André P., 1994, *MNRAS*, 268, 276
- Wilking B. A., Lada C. J., 1983, *ApJ*, 274, 698
- Wilking B. A., Lada C. J., Young E. T., 1989, *ApJ*, 340, 823
- Wootten A., 1989, *ApJ*, 337, 858